Published version available at: https://doi.org/10.1016/j.combustflame.2021.111731

Analytical study of superadiabatic small-scale combustors with a two-step chain-branching chemistry model: lean burning below the flammability limit

Javier Bosch, Daniel Fernández-Galisteo, Carmen Jiménez, Vadim N. Kurdyumov

Department of Energy, CIEMAT, Avda. Complutense 40, 28040 Madrid, Spain

Abstract

A study of combustion in small-scale superadiabatic burners with a counter-flow heat exchange segment is presented for a simple two-step chain-branching chemistry model. The work is focused on the possibility of burning below the flammability limit. The investigation is carried out in the high activation energy limit on the basis of analytical solutions. The existence of multiple steady-state regimes is demonstrated and their stability properties are investigated. These analytical results are finally compared with the results of numerical simulations carried out for finite activation energies.

1 Introduction

The design of near-limit chemical processes has wide technological applications, but very often their practical implementation turns out to be impossible without preheating or without adding other combustible substances. Among these applications, one can point out the chemical destruction of substances harmful to the environment, or fuel reforming processes, in which products needed for further use (for example, hydrogen) are obtained as a result of the partial oxidation of initial high molecular weight substances in an oxygen-lean process. However, the practical implementation of these and other similar processes becomes possible without additional energy costs in small-scale burners of the superadiabatic type, in which the temperature in the operational zone results to be significantly higher than the temperature obtained from a simple energy balance of the corresponding chemical transformations.

The study of superadiabatic burners has received considerable attention from experimental, theoretical and numerical points of view. Comprehensive reviews regarding these small-scale combustion devices can be found in [1–6] and in a very recent survey [7]. The underlying idea of this sort of devices based on heat recirculation should be traced back to [8–10] and over the past two decades a significant number of investigations on this subject have been reported [11–22].

An example of these superadiabatic burners is a system of parallel channels, where the reacting mixture moves in countercurrent flow. Despite the clear operational advantages that allow self-sustained chemical reactions without additional energy investment, the operation of such systems is subject to undesirable effects, such as possible extinction or instabilities, if the parameters are inadequately selected. This is due to the fact that a necessary characteristic of these devices is a small transverse scale of the operational zone, to allow efficient heat exchange between the channels. But the smallness of the characteristic dimensions decreases the volume-to-surface ratio, thus increasing possible heat losses. The investigation of these features to determine the range of parameters favorable for stable functioning is therefore a decisive part in the design of superadiabatic combustion devices.

It is worth mentioning that other types of devices - such as porous media - allow attaining temperatures in the reaction zone larger than the equilibrium temperature reached downstream. Such systems have been investigated in the past, see [23, 24], and more recently [25].

Most of the theoretical and numerical studies on combustion in superadiabatic devices were carried out either on the basis of a simplified one-step Arrhenius-type kinetics [12–15, 17, 18, 20, 22], or using complex kinetic schemes for specific chemical processes, as in [16, 19, 21]. In the case of Arrhenius kinetics, no flammability limit can be determined (a planar flame always exists for any fuel concentration within this kinetics). In the case of a complex kinetic scheme, it is difficult to reveal explicitly and with precision the flammability limit condition, if it exists at all. Nevertheless, the study of the interaction of the limiting flammability conditions and the thermophysical characteristics of a small-sized device is extremely important for better understanding its functioning principles.

A convenient kinetic scheme to study this issue is the simplified chain-branching reaction kinetics proposed by Zel'dovich [26–28]. In this mechanism, an initial fuel F is transformed into an intermediate radical Z by means of a thermally sensitive autocatalytic step, $F+Z \rightarrow 2Z$, with a finite activation energy. The radical species, being metastable, recombine into products P in an exothermic completion step, $2Z + M \rightarrow P + M + Q$, with M being any type of molecule. This chain-branching chemistry model was referred by Zeldovich as an idealized case of the hydrogen-oxygen combustion [27]. This mechanism was explored later by Liñán [29] using the high activation energy asymptotic (HAEA) limit where fast, intermediate and slow recombination regimes were identified. Sometimes this model is referred in the literature as the Zeldovich-Liñán (ZL) model. The HAEA analysis was carried out in [30] where non-zero heat release was assumed also for the autocatalytic step.

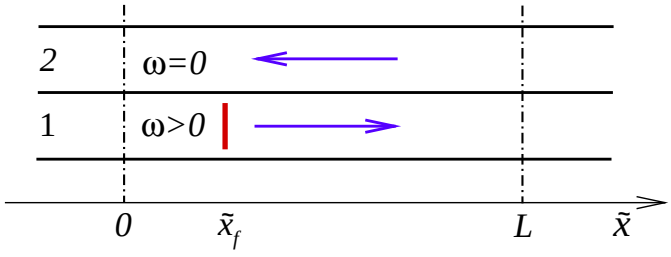

Figure 1: Sketch of the microburner configuration. Heat exchange between the channels takes place within segment $0 < \tilde{x} < L$. Arrows indicate gas flow directions and the vertical bold line indicates a flame located at $\tilde{x}_f$.

The above mechanism was modified by Dold et al. [31–34], where the completion step was suggested in the form $Z + M \rightarrow P + M$. The main difference between the original ZL-model and Dold's modification is the linearity of the completion reaction step with respect to the radical mass fraction. This results in the existence of a chain-branching crossover temperature, T_c, below which the rate of removal of the radical by diffusion is superior to the rate of chain-branching. This kinetic scheme was subsequently used for the numerical and asymptotic analysis of the structure and stability of flames [35–43]. The existence of a crossover temperature was shown in [44–46] for reduced hydrogen-oxygen kinetics. A detailed overview of these problems and their applications, along with a detailed discussion, can be found in [47].

The purpose of the present work is to show explicitly the possibility of implementing a self-sustaining combustion process for extremely lean mixtures below the flammability limit in a superadiabatic device. To this end, the modified kinetics proposed by Dold et al. [31–34] is used. According to the authors' knowledge, such an analysis has not yet been reported on this topic. The article is arranged as follows: the general formulation is presented in Section 2; the analytical treatment of steady-state solutions obtained in the high activation energy limit is developed in Section 3; the asymptotic treatment of a long channel case is presented in Section 4; the stability analysis of these steady state solutions is presented in Section 5, also on the basis of analytical solutions; finally, a comparison of the HAEA analytical and numerical solutions calculated for finite activation energies is presented in Section 6 and Section 7 contains the conclusions. In addition, the flammability limits development for the large activation energy case is given for completeness in the Appendix.

2 General formulation

A schematic representation of the combustion device investigated in the present work is given in Fig. 1. A combustible mixture flows in one channel where the combustion process takes place. The adjacent channel contains a chemically inert gas flowing in the opposite direction, which serves only to transfer heat. A similar type of device was considered in [18]. The mixture is assumed to be deficient in fuel while the mass fraction of the oxidizer, which is in abundance, remains nearly constant. The initial temperatures of both gases are equal to T_0 and the initial mass fraction of the combustible substance is F_0.

We assume that heat exchange between the channels takes place within a section of length L. Anticipating the results presented below, it should be noted in advance that the thermal conditions outside the heat-exchange section become of little importance if its length is large enough. In this study, we consider two opposite cases. In the first case, adiabatic conditions for $\tilde{x} < 0$ and $\tilde{x} > L$ are assumed in both channels. In the second case we consider the limiting situation when heat exchange with the external environment is very intense, so that for $\tilde{x} < 0$ and $\tilde{x} > L$ the gas temperatures in the two channels remain equal to the initial (cold) temperature T_0. Here and below " $\sim$ " is used to denote dimensional variables if the same notation is used for dimensional and dimensionless variables.

The two-step chain-branching kinetic mechanism used in the present study is identical to that explored in [31–41]. This chemistry includes the autocatalytic and recombination steps as follows

$$\begin{array}{lcl} F + Z \to 2Z & : & \Omega_B = A_B(\rho F/W_F)\cdot(\rho Z/W_Z)\,\exp\{-E/R_gT\}, \\ Z + M \to P + M + Q & : & \Omega_C = A_C(\rho Z/W_Z)\cdot(\rho/W), \end{array} \tag{1}$$

where Ω_B is the chain-branching reaction rate, assumed to be thermally sensitive with activation energy E, and Ω_C is the completion reaction rate with zero activation energy. As usual, all the heat, Q, is released in the completion step. In Eq. (1) A_B and A_C represent the reaction rate constants, ρ is the density, T is the temperature, F and Z are the mass fractions of fuel and radicals, R_g is the universal gas constant, and W_F, W_Z and W are the fuel, radical and mean molecular weights, respectively.

For the sake of simplicity, the present study deals with a diffusive-thermal model, according to which the density of the mixture ρ, the heat capacity c_p, the thermal conductivity, λ, and the molecular diffusivities of the fuel and radical species in the mixture, $\mathcal{D}_F$, $\mathcal{D}_Z$, are all constant. $\mathcal{D}_T = \lambda/\rho c_p$ stands for the thermal diffusivity, and is also constant within this model. The effects

of changes in density and transport properties with temperature will be discussed elsewhere.

In what follows, subindexes 1 and 2 are used to identify the channels with rightward and leftward flow directions, respectively, as sketched in Fig. 1. The analysis presented below is restricted to cases where the flow rates in the two channels are equal, i.e. $U_1 = -U_2 = U$. Thermo-physical properties of gases in both channels are assumed to be also identical. Within the one-dimensional approximation applicable to sufficiently thin channels, see [22], the conservation equations of species and energy take the form

$$\rho\left(\frac{\partial F}{\partial \tilde{t}} + U\frac{\partial F}{\partial \tilde{x}}\right) = \rho\mathcal{D}_F\frac{\partial^2 F}{\partial \tilde{x}^2} - W_F\Omega_B \tag{2}$$

$$\rho\left(\frac{\partial Z}{\partial \tilde{t}} + U\frac{\partial Z}{\partial \tilde{x}}\right) = \rho\mathcal{D}_Z\frac{\partial^2 Z}{\partial \tilde{x}^2} + W_Z\Omega_B - W_Z\Omega_C \tag{3}$$

$$\rho c_p\left(\frac{\partial T_1}{\partial \tilde{t}} + U\frac{\partial T_1}{\partial \tilde{x}}\right) = \lambda\frac{\partial^2 T_1}{\partial \tilde{x}^2} + Q\,\Omega_C - \mathcal{H}, \tag{4}$$

$$\rho c_p\left(\frac{\partial T_2}{\partial \tilde{t}} - U\frac{\partial T_2}{\partial \tilde{x}}\right) = \lambda\frac{\partial^2 T_2}{\partial \tilde{x}^2} + \mathcal{H}, \tag{5}$$

where $\tilde{x}$ and $\tilde{t}$ are the space and time variables and $\mathcal{H}$ is the heat-exchange term.

It is assumed that the heat-exchange term $\mathcal{H}$ has the form

$$\mathcal{H} = B\sigma(\tilde{x}/L)(T_1 - T_2), \tag{6}$$

where

$$\sigma(\zeta) = \begin{cases} 1, & 0 < \zeta < 1\,, \\ 0, & \zeta < 0, \quad \text{and} \quad \zeta > 1\,, \end{cases} \tag{7}$$

and B is the effective heat exchange parameter.

A dimensionless temperature is defined here as $\theta = (T - T_0)/(T_c - T_0)$. This choice is based on the branching temperature T_c, which takes into account the amount of radical removed by diffusion from the inner branching zone. This temperature is usually known as an "inhomogeneous" crossover temperature and has been widely discussed in [31–34]. The branching temperature T_c is determined by the relation $\Omega_B = \beta^2\Omega_C$ evaluated at the initial fuel mass fraction F_0, where $\beta = E(T_c - T_0)/R_gT_c^2$ is the Zel'dovich number based on T_c. It is important to see that the radical mass fractions Z in Ω_B and Ω_C are canceled out and, finally, T_c is defined by the equation

$$\frac{A_B}{A_C}\frac{W}{W_F}F_0 = \left\{\frac{E}{R_g}\cdot\frac{T_c - T_0}{T_c^2}\right\}^2 \exp\left\{\frac{E}{R_gT_c}\right\}. \tag{8}$$

In determining the dimensionless length and time parameters in combustion systems, the thermal flame width and the planar flame propagation velocity are often used. It should be noted that these quantities always exist in the case of a standard one-step kinetic model of the Arrhenius type, within which there is no flammability limit. However, in the case of chain-branching kinetics, these parameters may not exist when the initial fuel mass fraction is low, that is, in the case of a mixture below the flammability limit. This means that the adiabatic temperature, namely the temperature obtained during complete fuel burning in a planar flame without heat-losses, remains below the branching temperature. These are the cases where the application of superadiabatic devices is of particular interest.

Because we are interested in these cases where a flame width and propagation speed can not be defined, the characteristic time and length, t_c and L_c, used to define the dimensionless variables $x = \tilde{x}/L_c$ and $t = \tilde{t}/t_c$ are chosen from the following relations

$$t_c \mathcal{D}_T/L_c^2 = 1, \quad t_c \rho A_C/W = 1. \tag{9}$$

The first relation is obtained by equating the orders of magnitude of the unsteady and diffusion terms in Eq. (4). The second relation is determined from equating the unsteady and the completion reaction terms in Eq. (3). The characteristic quantities L_c and t_c determine the scale of the characteristic velocity $U_c = L_c/t_c = \sqrt{\rho A_C \mathcal{D}_T/W}$.

Using F_0 and $Z_0 = (W_Z/W_F)F_0$ to normalize the mass fractions of fuel and radicals, respectively, the dimensionless counterparts of Eqs. (2)-(5) take the form

$$\frac{\partial F}{\partial t} + m\frac{\partial F}{\partial x} = \frac{1}{Le_F}\frac{\partial^2 F}{\partial x^2} - \omega\,, \tag{10}$$

$$\frac{\partial Z}{\partial t} + m\frac{\partial Z}{\partial x} = \frac{1}{Le_Z}\frac{\partial^2 Z}{\partial x^2} + \omega\, - Z, \tag{11}$$

$$\frac{\partial \theta_1}{\partial t} + m\frac{\partial \theta_1}{\partial x} = \frac{\partial^2 \theta_1}{\partial x^2} + qZ - b\,\sigma(x/\ell)(\theta_1 - \theta_2)\,, \tag{12}$$

$$\frac{\partial \theta_2}{\partial t} - m\frac{\partial \theta_2}{\partial x} = \frac{\partial^2 \theta_2}{\partial x^2} + b\,\sigma(x/\ell)(\theta_1 - \theta_2)\,, \tag{13}$$

where

$$\omega = \beta^2\, F\, Z\, \exp\left\{\frac{\beta(\theta_1 - 1)}{1 + \gamma(\theta_1 - 1)}\right\}. \tag{14}$$

Here b is the dimensionless intensity of heat exchange between channels, defined below, $\ell = L/L_c$ is the dimensionless length of the heat exchange segment, $m = U/U_c$ is the dimensionless flow velocity, $q = QF_0/c_p(T_c - T_0)W_F$ is the dimensionless heat of reaction, $\gamma = (T_c - T_0)/T_c$

is the heat release parameter, $Le_F = \mathcal{D}_T/\mathcal{D}_F$ and $Le_Z = \mathcal{D}_T/\mathcal{D}_Z$ are the Lewis numbers of the fuel and radicals.

The calculation of the dimensionless heat exchange parameter b within the narrow channel approximation is detailed in [22]. The only difference introduced in this work is the need to replace the thermal width of the flame δ_T (which may not exist for cases below the flammability limit) by L_c. The final expression takes the form

$$b = \alpha \frac{\lambda_w}{\lambda} \frac{L_c^2}{H H_w}\,, \tag{15}$$

where H and H_w are the channel and wall widths, respectively, and λ_w is the wall thermal conductivity. The dimensionless factor α depends on the configuration of the burner: if a periodic array of channels is considered, as is done in [22], then $\alpha = 2$. If we consider only two channels with external lateral adiabatic walls thermally isolating from the external environment, then $\alpha = 1$.

The following boundary conditions are applied. For the mass fractions of fuel and radicals, we use

$$x \to -\infty: \quad F - 1 = Z = 0, \quad x \to \infty: \quad \partial F/\partial x = \partial Z/\partial x = 0\,. \tag{16}$$

For the temperature field, two types of conditions will be used. In the first case, where heat losses outside the heat exchange segment are neglected (adiabatic walls), we assume

$$x \to -\infty:\ \theta_1 = \partial\theta_2/\partial x = 0; \quad x \to -\infty:\ \theta_2 = \partial\theta_1/\partial x = 0\,. \tag{17}$$

In the second case, where very fast heat exchange with the external environment is assumed and the temperature becomes close to the initial temperature for $x < 0$ and $x > \ell$, we impose

$$x = 0,\, \ell: \quad \theta_1 = \theta_2 = 0\,. \tag{18}$$

The flame position, x_f, is defined below as a point where the temperature is equal to the branching temperature, $\theta_1(x_f) = 1$. This point is close to that where the radical mass fraction Z reaches its maximum value. In the limiting HAEA case considered below, these points coincide. Nevertheless, it should be noted that at finite β, the branching temperature becomes slightly smaller than unity, so that the unit temperature in the channel may not be attained. In these cases, the point with the maximum concentration of radicals is used for the flame position.

Taking into account that the molecular weight of the radicals is usually smaller than the molecular weight of the initial substances, the case of $Le_z = 0.3$ will be considered below,

unless otherwise indicated. It should also be noted that the steady-state results do not depend, or only slightly depend (at finite β), on the Lewis number for the initial fuel, Le_F. This fact is not new and was noted in [31–34] for the modified ZL-model. In contrast, the stability results depend on the fuel Lewis number.

3 Analytical steady-state solutions for $\beta \gg 1$

In the HAEA limit, $\beta \gg 1$, the radical production term is reduced to the Dirac δ-function located at the point where $\theta_1 = 1$, namely $\omega \sim \delta(x - x_f)$ and x_f is the flame-sheet position, see [31–34]. The jump conditions for variables across the flame sheet take the form

$$\big[Z\big] = \big[F\big] = Le_F^{-1}\big[F^I\big] + Le_Z^{-1}\big[Z^I\big] = 0, \tag{19}$$

$$\theta_1|_{x_f-} = \theta_1|_{x_f+} = 1, \quad \big[\theta_2\big] = \big[\theta_1^I\big] = \big[\theta_2^I\big] = 0\,, \tag{20}$$

where $[f] = f(x_f + 0) - f(x_f - 0)$ and f^I denotes a derivative with respect to x. These jump conditions for variables and derivatives are obtained by combining the equations and integrating over the flame sheet.

Imposing $\partial/\partial t \equiv 0$ and assuming that at $x = x_f$ the fuel is consumed completely, the steady-state solutions of Eq. (10)-(11) take the form

$$F = \begin{cases} 1 - \exp\left[Le_F\, m\,(x - x_f)\right], & x < x_f\,, \\ 0, & x > x_f\,. \end{cases} \tag{21}$$

$$Z = \begin{cases} Z_f \exp[a_m(x - x_f)], & x < x_f\,, \\ Z_f \exp[a_p(x - x_f)], & x > x_f\,, \end{cases} \tag{22}$$

where

$$a_m = \frac{Le_Z m + \sqrt{Le_Z^2 m^2 + 4Le_Z}}{2}\,, \quad a_p = \frac{Le_Z m - \sqrt{Le_Z^2 m^2 + 4Le_Z}}{2}\,, \tag{23}$$

and

$$Z_f = \frac{m Le_Z}{\sqrt{Le_Z^2 m^2 + 4Le_Z}} \tag{24}$$

is obtained from the jump conditions given by Eq. (19). Note that regardless of the boundary conditions selected for the temperature at $x < 0$ and $x > \ell$, the solutions given by Eqs. (21)-(24) for the mass fractions remain the same.

The equations to determine the steady-state temperature distributions in both channels become

$$\begin{cases} m\theta_1^I = \theta_1^{II} + qZ - b\,\sigma(x/\ell)(\theta_1 - \theta_2)\,, \\ -m\theta_2^I = \theta_2^{II} + b\,\sigma(x/\ell)(\theta_1 - \theta_2)\,, \end{cases} \tag{25}$$

For the sake of completeness, the calculation of the flammability limit condition, defined as the value of $q = q_f$ below which a planar adiabatic freely propagating flame can not exist, is given in the Appendix for the case of large β. This issue was discussed for the first time in [31]. It was shown that $q_f = 1$ is obtained independently of the Lewis numbers within the HAEA limit.

3.1 No heat losses outside the heat-exchange segment

Let us consider first the case of adiabatic conditions for $x < 0$ and $x > \ell$. Equations (25) are to be solved with the boundary conditions given by Eq. (17). Because the heat-exchange term is zero for $x < 0$ and $x > \ell$, the solution for the temperature field outside the heat-exchange segment becomes

$$\theta_1 = \begin{cases} A_1 e^{m\,x} + \dfrac{qZ_f}{ma_m - a_m^2} e^{a_m(x - x_f)}\,, & x < 0, \\ A_2 + \dfrac{qZ_f}{ma_p - a_p^2} e^{a_p(x - x_f)}\,, & x > \ell, \end{cases} \quad \theta_2 = \begin{cases} A_3\,, & x < 0, \\ A_4 e^{-m\,x}\,, & x > \ell, \end{cases} \tag{26}$$

where A_i, $i = 1, \ldots 4$ are unknown constants. Eq. (26) allows to write the following conditions independent of A_i

$$\begin{aligned} x = 0: \quad & m\theta_1 - \theta_1^I = qZ_f \frac{m - a_m}{ma_m - a_m^2}\, e^{-a_m x_f}, \qquad && \theta_2^I = 0\,, \\ x = \ell: \quad & \theta_1^I = qZ_f \frac{a_p}{ma_p - a_p^2}\, e^{a_p(\ell - x_f)}, && m\theta_2 + \theta_2^I = 0\,. \end{aligned} \tag{27}$$

Thus, the problem of finding the temperatures in the two channels is reduced to solving Eq. (25) separately for $0 < x < x_f$ and $x_f < x < \ell$ followed by application of the conditions on the flame sheet. The total number of conditions is nine: five conditions provided by Eq. (20) and four by Eq. (27).

Equations (25) written on both sides of the flame sheet are linear and have an analytical solution containing eight constants, $\{C_i,\, i = 1, \ldots 8\}$, four on each side. These constants are determined from any eight conditions given by (20) and (27), which requires solving a system of eight linear inhomogeneous equations. The remaining ninth condition providing a solvability

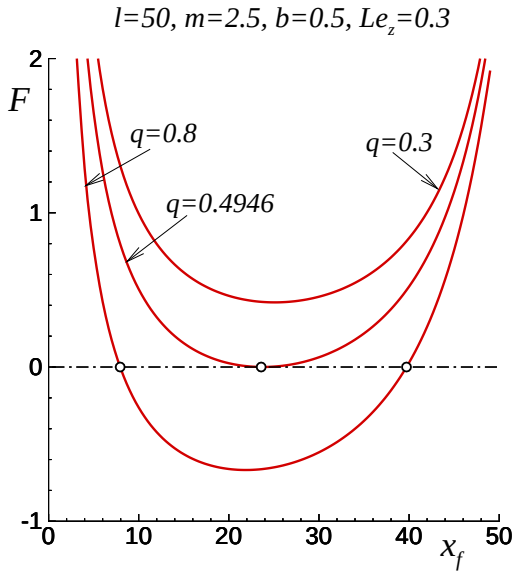

Figure 2: Typical examples of the function $\mathcal{F}$ of Eq. (28) with two, one and zero roots.

condition of the form

$$\mathcal{F}(x_f; m, q, \ell, b, Le_z) = 0 \tag{28}$$

is applied to determine the flame position, x_f. This analytical procedure was carried out using MAPLE, which facilitates the algebraic steps tremendously. Although this leads to an analytical expression for $\mathcal{F}$, this is a very long expression with no way to be written explicitly in this article. In addition, it does not reveal much about the nature of the solution. Typical examples of the function $\mathcal{F}$ plotted versus x_f are shown in Figure 2, where one can see the cases with two, one and no roots. The intermediate one-root case corresponds to a critical event where two roots merge into one and then disappear. The exhaustive parametric study presented below is based on the numerical evaluation of the analytical expression for $\mathcal{F}$.

The calculated values of x_f are presented in Fig. 3 as a function of q. The left plot shows the curves evaluated for $\ell = 50$ and different values of the heat transfer coefficient b. The right figure shows the values of x_f obtained for $b = 0.5$ and various values of ℓ. It can be seen in the left plot that for very lean mixtures, $q < 1$, steady-state solutions exist for a sufficiently large heat transfer coefficient b when the length ℓ is fixed. The right plot shows that when the coefficient b is fixed, an increase in ℓ also leads to the appearance of combustion modes for $q < 1$. Anticipating the results presented in Section 5, it should be noted that the solution with a larger value of x_f is unstable.

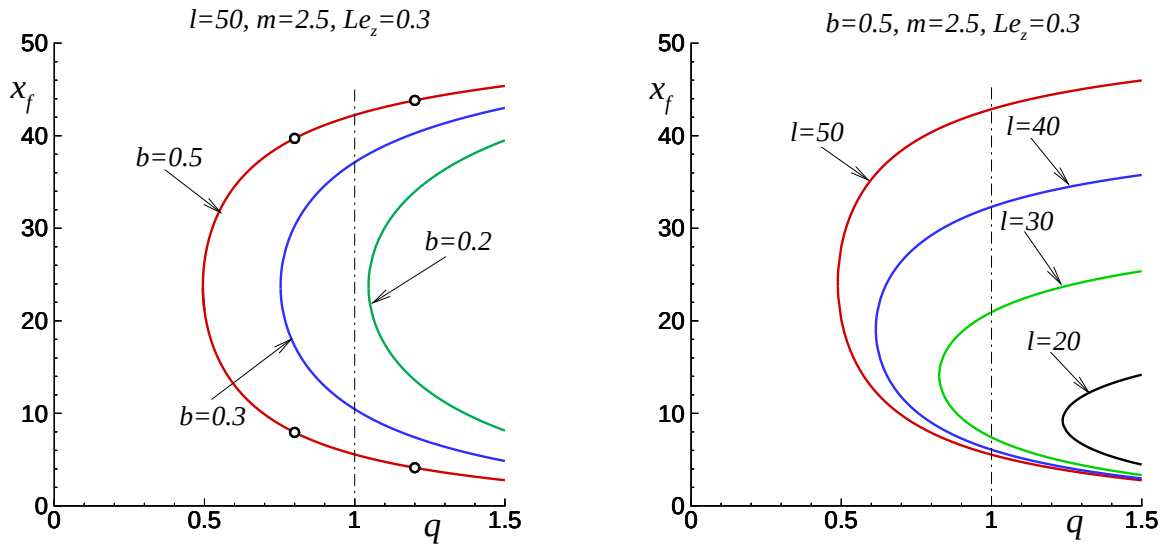

Figure 3: Dependence of the combustion front position x_f versus the dimensionless heat of reaction q for different b values (left plot) and different ℓ values (right plot). Open circles in the left plot correspond to the distributions shown in Fig. 4. The vertical dash-dotted lines indicate the standard flammability limit $q_c = 1$.

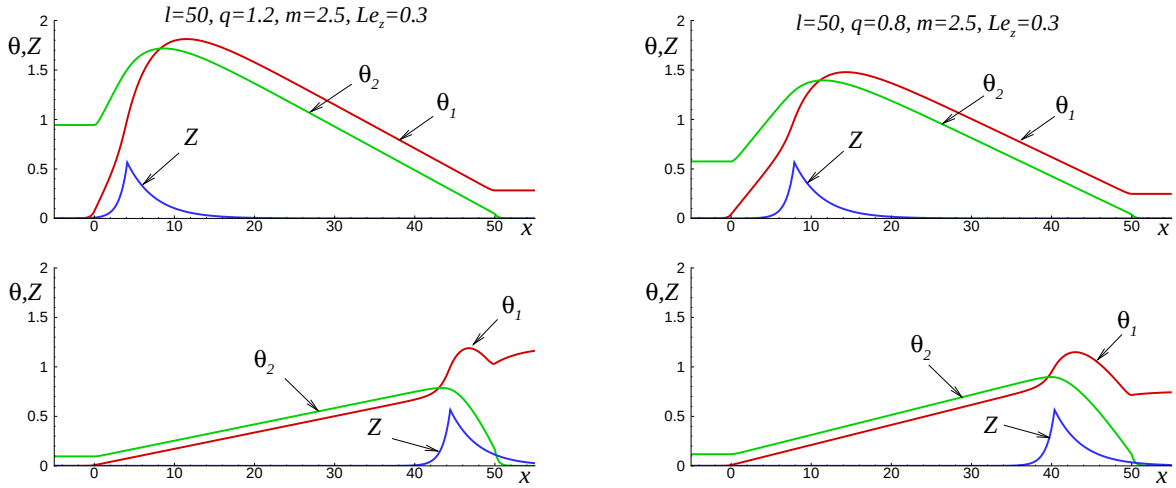

Figure 4: Examples of the temperature distributions in the two channels (θ_1 for the reacting channel and θ_2 for the non-reacting gas) and the distribution of radicals Z for the four steady-state solutions marked with open circles in Fig. 3.

Typical temperature and mass fraction distributions are illustrated in Fig. 4 for the cases of

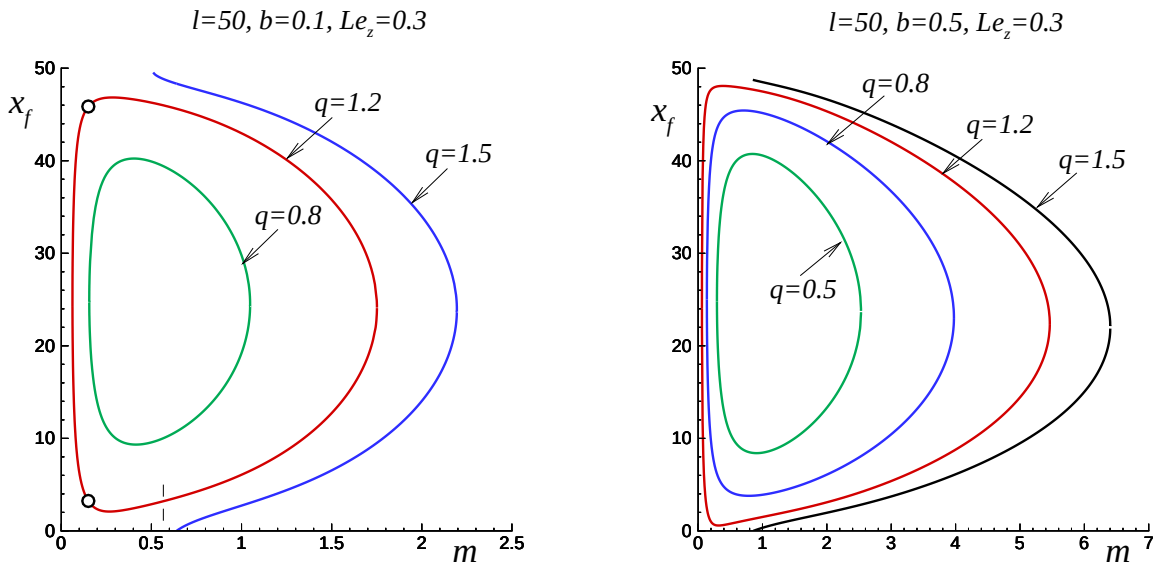

Figure 5: Dependence of the combustion front position x_f versus the dimensionless flow rate m for several values of q. Open circles correspond to the distributions shown in Fig. 6.

mixtures richer than the flammability limit ($q > 1$, left plots) and leaner than the flammability limit ($q < 1$, right plots). These distributions correspond to the open circles shown in Fig. 3 (left).

Figure 5 shows the dependence of the flame position on the flow rate m for different values of q. The left picture shows cases with $b = 0.1$, the right one with $b = 0.5$. One can see that there is always a maximum flow rate above which there are no solutions. For $q < 1$, the curves in the figure are closed. However, with an increase in q, it can be seen that x_f approaches the edge of the heat-exchange zone when the flow rate decreases. Obviously, at $q > 1$ unsteady regimes exist in which the combustion wave propagates upstream in the adiabatic segment $x < 0$. These dynamical modes exist at values $m < m_c$, where m_c is determined from Eq. (50). The value of m_c calculated for $q = 1.2$ is marked with a vertical dashed line in the left plot of this figure. Nevertheless, the curves plotted for $q = 1.2$ in Fig. 5 shows that steady-state solutions with $0 < x_f < \ell$ can also exist simultaneously. The temperature distributions for this kind of steady-state solutions are exemplified in Fig. 6 corresponding to the open circles shown in Fig. 5 (left).

It should be noted that the general structure of the solutions obtained for the chain-branching kinetics resembles to some extent that obtained by other authors for the case of either one step Arrhenius or detailed chemical kinetics. For example, similar closed response curves were also

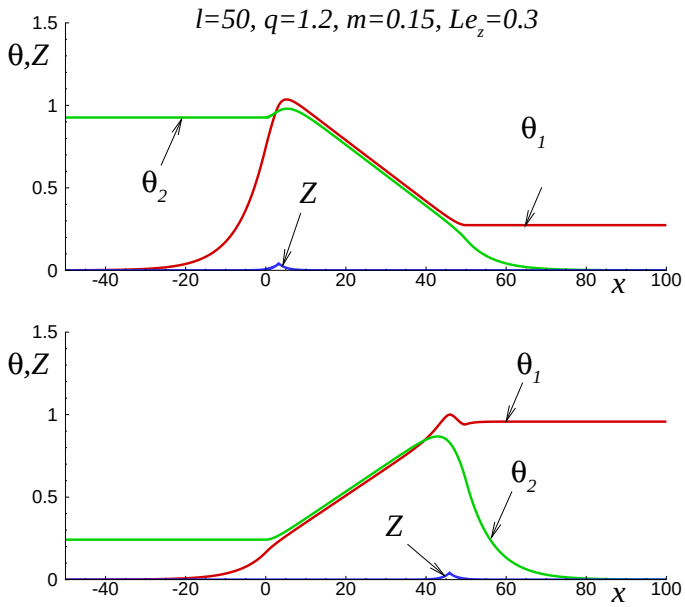

Figure 6: The temperature distributions in the two channels (θ_1 for the reacting channel and θ_2 for the non-reacting channel) and the distribution of radicals Z corresponding the points marked with open circles in Fig. 5. These solutions exist simultaneously with a time-dependent solution corresponding to the flame propagating upstream.

found, for instance, in [13, 14, 21] for the flame-sheet simplification of Arrhenius kinetics. The existence of a multiplicity of steady-state solutions was demonstrated in various studies, e.g. [21, 22, 25]. The limitation on the values of the flow rate was also noted by different authors. These general features are associated with the peculiarities of the heat transfer process (heat recirculation) in super adiabatic devices. However, the main new result of the present work is that for the first time the feasibility of steady combustion for extremely lean mixtures below the flammability limit is explicitly demonstrated. According to the knowledge of the authors, this has not been demonstrated before.

3.2 Isothermal (cold) conditions for $x < 0$ and $x > \ell$

In the limiting case of intensive heat losses applied for $x < 0$ and $x > \ell$, the procedure to solve Eqs. (25) remains the same as described above. The only difference is that Eq. (18) is applied instead of Eq. (17). Figure 7 compares the cases where the segments $x < 0$ and $x > \ell$ are isothermal (solid lines) and adiabatic (dashed lines). It can be seen that a change in boundary

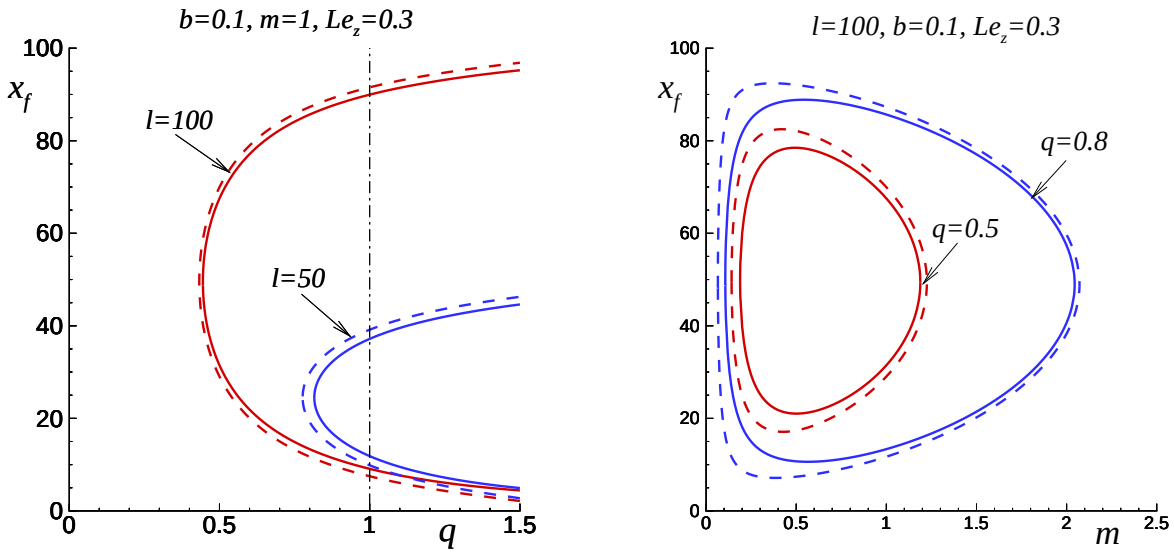

Figure 7: Comparison of the dependencies of x_f on q (left plot) and x_f on m in the cases of isothermal (solid lines) and adiabatic (dashed lines) assumptions for the wall for $x < 0$ and $x > \ell$.

conditions at the entrance of the heat-exchange section leads only to slight variations in the steady-state results. The difference also decreases with an increase of the heat exchange section length. The asymptotic considerations for the limiting case $\ell \gg 1$ are presented in the next Section.

Obviously, the steady-state solutions obtained within the HAEA limit cannot depend on Le_F, since this parameter disappears from the conditions at the flame sheet, and, thus, from the final analytical steady-state expressions. Up to this point, all the results presented have been reported for $Le_Z = 0.3$. Figure 8 compares the curves obtained for different values of Le_Z calculated with the isothermal conditions at $x < 0$ and $x > \ell$. One can see in this figure that the influence of Le_Z is extremely small. Apparently, this can be explained by the fact that the impact of the Lewis number on the flame structure is important in cases of curved flames, which is not the case of the present study.

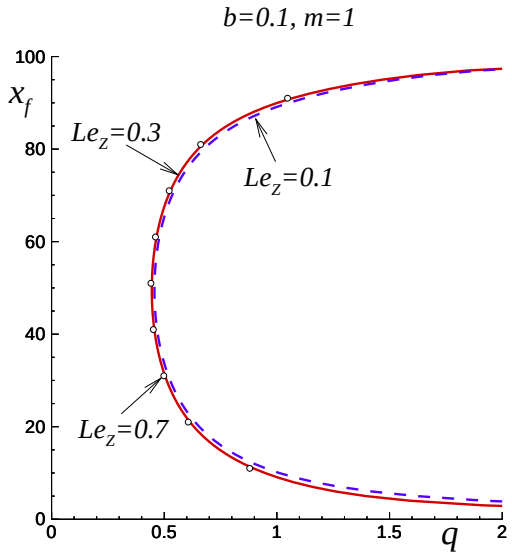

Figure 8: Comparison of the dependencies for x_f on q for different Lewis numbers Le_z, for $\ell = 100$, $m = 1$ and $b = 0.1$.

4 Asymptotic solution for $\ell \gg 1$

The solutions presented in Section 3 were obtained analytically. However, their analysis is extremely difficult due to the length of the resulting formulae that would fill several pages. The asymptotic approximation presented below helps to understand better the general structure of the solutions. An additional purpose of considering this limit is to validate the analytical results obtained in the previous Section.

Consider the limit of a long heat-exchange segment, $\ell \gg 1$. We assume also that $b = \hat{b}/\ell$, where $\hat{b}$ is considered to be (formally) of order unity. To solve Eqs. (25), the method of matched asymptotic expansions is applied [48]. To do this, as usual, the inner and outer variables are introduced as follows: $\eta = x - x_f$ for the inner variable and $\xi = (x - x_f)/\ell$ for the outer variable. The internal and external variables for the temperature are denoted as $\theta^{in}(\eta)$ and $\theta^{out}(\xi)$, respectively. The first order matching conditions read

$$\lim_{\xi\to 0-} \theta_1^{out}(\xi) = \lim_{\eta\to-\infty} \theta_1^{in}(\eta)\,, \quad \lim_{\xi\to 0+} \theta_1^{out}(\xi) = \lim_{\eta\to\infty} \theta_1^{in}(\eta)\,. \tag{29}$$

The inner region corresponds to $|\eta| = O(1)$. Taking into account that $b = \tilde{b}/\ell$, the heat-exchange term is small in the inner region, to the leading order. Thus, the solution of Eqs. (25)

for θ_1^{in} is given by

$$\theta_1^{in}(\eta) = \begin{cases} c_1 + c_2 e^{m\eta} + \dfrac{qZ_f}{ma_m - a_m^2} e^{a_m \eta}\,, & \eta < 0\,, \\ c_3 + c_4 e^{m\eta} + \dfrac{qZ_f}{ma_p - a_p^2}\, e^{a_p \eta}\,, & \eta > 0\,, \end{cases} \tag{30}$$

where a_p, a_m and Z_f are given by Eqs. (23)-(24).

Rewriting this inner solution in terms of the outer variable $\xi = O(1)$ indicates that $c_4 = 0$ should be imposed in order to eliminate the corresponding exponentially large term, namely the term $\sim c_4 e^{\ell\, m\, \xi}$ growing exponentially for positive $\xi = O(1)$ and $\ell \gg 1$. Applying conditions (20) written at $\eta = 0$,

$$\theta_1^{in}(0+) = \theta_1^{in}(0-) = 1, \quad [d\theta_1^{in}/d\eta] = 0\,,$$

gives

$$\begin{aligned} c_1 &= 1 - \frac{qZ_f}{m}\left\{ \frac{m - a_m}{ma_m - a_m^2} + \frac{a_p}{ma_p - a_p^2} \right\} \\ c_2 &= \frac{qZ_f}{m}\left\{ \frac{a_p}{ma_p - a_p^2} - \frac{a_m}{ma_m - a_m^2} \right\} \\ c_3 &= 1 - \frac{qZ_f}{ma_p - a_p^2} \end{aligned} \tag{31}$$

Thus, from Eq. (30) it follows that

$$\lim_{\eta \to -\infty} \theta_1^{in}(\eta) = \theta_1^{(-)}, \quad \lim_{\eta \to +\infty} \theta_1^{in}(\eta) = \theta_1^{(+)}\,, \tag{32}$$

where $\theta_1^{(-)} = c_1$ and $\theta_1^{(+)} = c_3$. It can be checked also that $\theta_1^{(+)} - \theta_1^{(-)} = q$, as it should be, and $\theta_1^{(-)} < 1$ and $\theta_1^{(+)} > 1$. These values are used for the matching procedure between the inner and outer solutions.

The leading order of Eqs. (25) written in terms of the outer variable takes the form

$$\begin{aligned} m\, d\theta_1^{out}/d\xi &= -\tilde{b}(\theta_1^{out} - \theta_2^{out})\,, \\ -m\, d\theta_2^{out}/d\xi &= \tilde{b}(\theta_1^{out} - \theta_2^{out})\,, \end{aligned} \tag{33}$$

because the radicals mass fraction Z given by Eq. (22) is exponentially small in the outer region $\xi = O(1)$. These equations are to be solved separately for $-\xi_f < \xi < 0$ and for $0 < \xi < 1 - \xi_f$, where $\xi_f = x_f/\ell$, to be found. The corresponding boundary and matching conditions are

$$\begin{gathered} \theta_1^{out}(-\xi_f) = 0, \quad \theta_2^{out}(1 - \xi_f) = 0, \\ \lim_{\xi \to 0-} \theta_1^{out}(\xi) = \theta_1^{(-)}, \quad \lim_{\xi \to 0+} \theta_1^{out}(\xi) = \theta_1^{(+)}, \quad \theta_2^{out}(0+) = \theta_2^{out}(0-)\,. \end{gathered} \tag{34}$$

Here the first two conditions represent the leading order of the boundary conditions obtained from Eq. (27) in the case of adiabatic segments. In the case of isothermal walls, these conditions are accurate.

The general solution of Eqs. (33) has the form

$$\theta_1^{out}(\xi) = \frac{C_1 + C_2}{2} - \frac{\tilde{b}}{m} C_1 \xi, \quad \theta_2^{out}(\xi) = \frac{C_2 - C_1}{2} - \frac{\tilde{b}}{m} C_1 \xi \,, \tag{35}$$

where C_1 and C_2 are arbitrary constants. Thus, there are four constants (two on each side of the flame) which are found by means of any four conditions from (34). The last fifth condition is used to determine the position of the flame. After these algebraic steps, the explicit expression for the flame position can be obtained. In terms of the external variable ξ_f, the result is

$$\xi_{f_{1,2}} = \frac{q\hat{b} \pm \sqrt{q[\hat{b}^2 q - 4\theta_1^{(-)} m(m+\hat{b})]}}{2q\hat{b}} \,, \tag{36}$$

where there are two roots and $\theta_1^{(-)}$ is determined by Eq. (32). Remember that $\xi_f = x_f/\ell$ and $\hat{b} = b \cdot \ell$.

Equation (36) allows us to find analytically the minimum value of q above which there are two solutions. This value corresponds to the point where the two roots of Eq. (36) are merged, $\xi_{f1} = \xi_{f2}$. We have

$$q_{min} = \frac{4m(m + b\,\ell)}{b^2\ell^2 + 4\alpha m(m + b\,\ell)} \,, \tag{37}$$

where

$$\alpha = \frac{Z_f}{m}\left\{\frac{m - a_m}{m a_m - a_m^2} + \frac{a_p}{m a_p - a_p^2}\right\}.$$

It can be seen from Eq. (37) that $q_{min} \sim \ell^{-1}$ as $\ell \gg 1$ for a fixed value of b and $q_{min} \sim b^{-1}$ for a fixed value of ℓ. It means that for any arbitrarily small q, there is a critical length of the heat exchange segment, ℓ_c, or a critical value of the heat-exchange parameter, b_c. Thus, combustion can be carried out having $q_{min} < q$ if $\ell > \ell_c$ or $b > b_c$. In other words, there is always a way of making the combustion process feasible, either by making the heat exchange segment longer or by making the heat exchange coefficient larger.

This asymptotic procedure helps to understand the structure of solutions for $\ell \gg 1$ and $b = O(1/\ell)$. In the inner region, $|x - x_f| = O(1)$, a thermal balance occurs between the diffusion and heat release terms. In the outer region, $|x - x_f|/\ell = O(1)$, a balance is established between the heat convection term and the heat-exchange term between the channels.

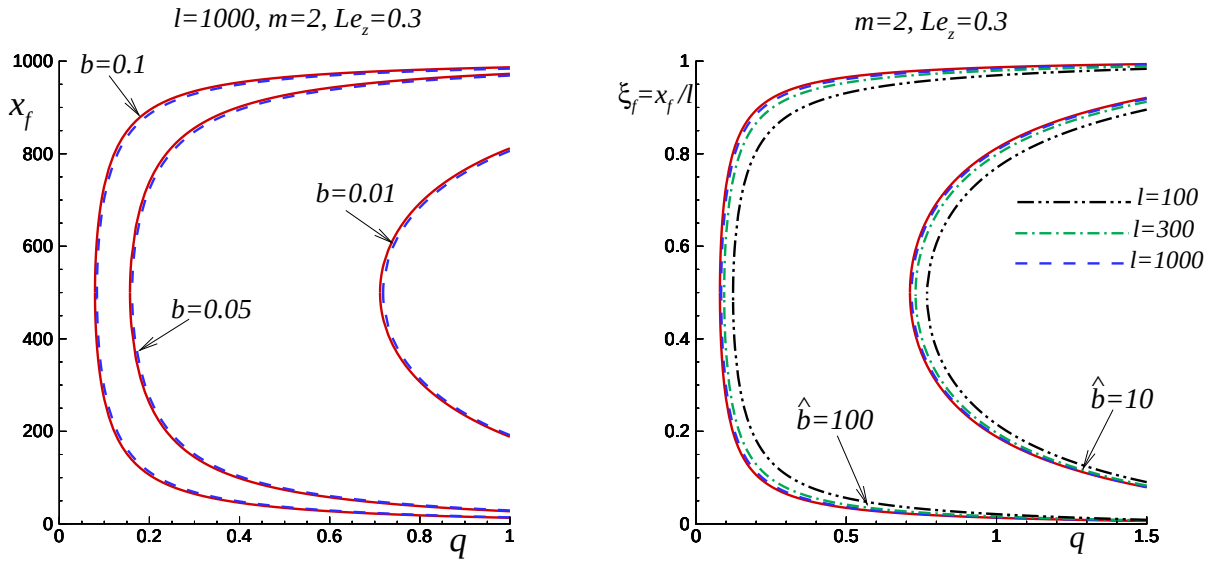

Figure 9: Left plot: the flame position x_f versus q for the general case (dashed lines) and the asymptotic approximation obtained for $\ell \gg 1$ (solid lines, plotted with $\tilde{b} = b \cdot \ell$). Right plot: the scaled flame position $\xi_f = x_f/\ell$ versus q for various ℓ; the solid lines shows the asymptotic results, the dashed, dash-dot and dash-dot-dot lines show the cases with $\ell = 1000$, 300 and 100, respectively, plotted for $\hat{b} = 100$ and $\hat{b} = 10$ (where $b = \hat{b}/\ell$ was applied).

Figure 9 (left) compares the flame position x_f versus q calculated using the asymptotic result given by Eq. (36) (solid lines) and the general analytical solutions developed in Section 3 (dashed lines) for $\ell = 1000$, $m = 2$, $Le_z = 0.3$ and various b. The right plot in Fig. 9 shows the dependence of the scaled flame position, $\xi_f = x_f/\ell$, as a function of q for two values of the scaled heat-exchange coefficient, $\hat{b} = 100$ and 10, and various ℓ. The solid line represents the asymptotic curve given by Eq.(36) while the dashed, dash-dot and dash-dot-dot lines show the general result obtained for $\ell = 1000$, 300 and 100, respectively, where the coefficient b calculated as $b = \hat{b}/\ell$ with $\hat{b}$ fixed at 100 and 10. This plot demonstrates convergence to the asymptotic result with increasing values of ℓ. The values of q_{min} given by Eq. (37) are plotted in Fig. 10 as a function of m for $\ell = 1000$ and various b where the standard flammability value $q_f = 1$ is indicated with a horizontal dash-dot line.

One can see also, that the requirement $b = O(\ell^{-1})$ made at the beginning of this analysis is necessary for the flame position to be at a distance $x_f = O(\ell)$ (in terms of the inner variable). Equation (36) shows that (formally) for $b = O(1)$, or equivalently for $\tilde{b} \gg 1$, the flame position

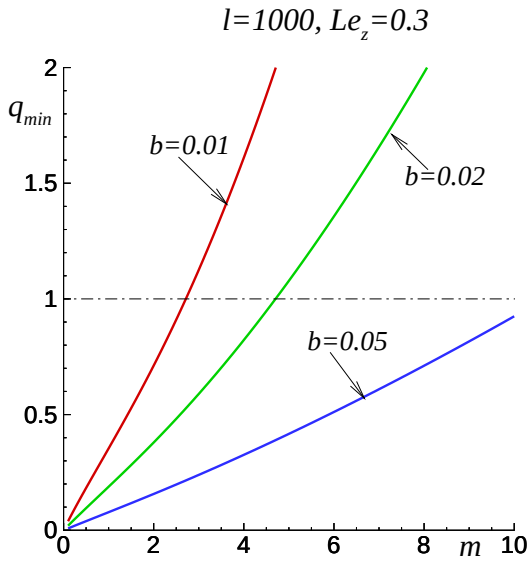

Figure 10: Dependence of q_{min} on the flow rate m calculated from Eq. (36); the dashed-dot horizontal line indicates the standard flammability limit and the combustion regimes exist for $q > q_{min}$.

x_f is located at a distance of the order of unity from the boundaries of the heat exchange segment.

5 Stability analysis

Stability analysis of the solutions presented in Section 3 is now performed. The steady-state distributions of the mass fractions, the temperatures in both channels and the steady-state flame position, all now denoted by subindex "0", are perturbed as usual with small perturbations

$$\begin{aligned} F &= F_0(x) + \epsilon \hat{F}(x) \exp(\lambda t), \\ Z &= Z_0(x) + \epsilon \hat{Z}(x) \exp(\lambda t), \\ \theta_1 &= \theta_{10}(x) + \epsilon \hat{\theta}_1(x) \exp(\lambda t), \\ \theta_2 &= \theta_{20}(x) + \epsilon \hat{\theta}_2(x) \exp(\lambda t), \\ x_f &= x_{f0} + \epsilon \exp(\lambda t), \end{aligned} \tag{38}$$

where $\lambda = \lambda_R + I\lambda_I$ is a complex number. The real part of λ represents the growth rate, and ϵ is a small amplitude. The aim of this section is to clarify if a given steady-state is stable or not, and not to construct a complete spectrum of eigenvalues. For this purpose, it is enough to find

out whether there are eigenvalues with $\lambda_R > 0$.

The linearized eigenvalue problem obtained when substituting Eqs. (38) into Eqs. (10)-(13) reduces to finding non-trivial solutions of the following system of equations

$$\begin{aligned} \lambda\hat{F} + m\hat{F}^I &= Le_F^{-1}\hat{F}^{II}\,, \\ \lambda\hat{Z} + m\hat{Z}^I &= Le_Z^{-1}\hat{Z}^{II} - \hat{Z}\,, \end{aligned} \tag{39}$$

$$\begin{aligned} \lambda\hat{\theta}_1 + m\hat{\theta}_1^I &= \hat{\theta}_1^{II} + q\hat{Z} - b\,\sigma(x/\ell)(\hat{\theta}_1 - \hat{\theta}_2)\,, \\ \lambda\hat{\theta}_2 - m\hat{\theta}_2^I &= \hat{\theta}_2^{II} + b\,\sigma(x/\ell)(\hat{\theta}_1 - \hat{\theta}_2)\,. \end{aligned} \tag{40}$$

These equations are to be solved on either side of the flame sheet.

The corresponding linearized conditions at the flame sheet obtained from Eq. (19)-(20) take the form

$$\begin{gathered} \left[Z_0^I + \hat{Z}\right] = 0\,, \quad \left[F_0^I + \hat{F}\right] = 0\,, \\ Le_F^{-1}\left[F_0^{II} + \hat{F}^I\right] + Le_Z^{-1}\left[Z_0^{II} + \hat{Z}^I\right] = 0\,, \end{gathered} \tag{41}$$

$$\begin{gathered} (\theta_{10}^I + \hat{\theta}_1)|_{x_{f0}-0} = 0\,, \quad (\theta_{10}^I + \hat{\theta}_1)|_{x_{f0}+0} = 0\,, \quad \left[\theta_{10}^{II} + \hat{\theta}_1^I\right] = 0\,, \\ \left[\theta_{20}^I + \hat{\theta}_2\right] = 0\,, \quad \left[\theta_{20}^{II} + \hat{\theta}_2^I\right] = 0\,, \end{gathered} \tag{42}$$

The boundary conditions at infinity for perturbations of mass fractions are

$$x \to \pm\infty: \quad \hat{F} = \hat{Z} = 0\,, \tag{43}$$

For simplicity, consider the case of isothermal segments for $x < 0$ and $x > \ell$ by imposing the following boundary conditions

$$x = 0, \ell: \quad \hat{\theta}_1 = \hat{\theta}_2 = 0\,. \tag{44}$$

The procedure for constructing solutions for perturbations is similar to that used to construct steady-state solutions. Let us use the following notation:

$$\begin{gathered} s = \sqrt{Le_Z[m^2 Le_Z + 4(\lambda+1)]} \quad p = \sqrt{Le_F[m^2 Le_F + 4\lambda]} \\ \tilde{b}_m = \frac{mLe_F + p}{2} \quad \tilde{a}_m = \frac{mLe_z + s}{2}\,, \quad \tilde{a}_p = \frac{mLe_z - s}{2} \\ D_1 = \frac{Le_Z m[(Le_F - Le_Z)m - s - p]}{2s}\,, \quad D_2 = D_1 + Le_Z\, m\,. \end{gathered}$$

Solutions for Eqs. (39) for $\hat{F}$ and $\hat{Z}$ subject to the conditions (41) and (43) can be written as follows

$$\hat{F} = \begin{cases} Le_F m\, e^{\tilde{b}_m(x-x_{f0})}\,, \\ 0\,, \end{cases} \quad \hat{Z} = \begin{cases} D_1\, e^{\tilde{a}_m(x-x_{f0})}\,, & x < x_{f0}\,, \\ D_2\, e^{\tilde{a}_p(x-x_{f0})}\,, & x > x_{f0}\,. \end{cases} \tag{45}$$

After that, an analytical solution for the temperature perturbation field was obtained with the help of MAPLE.

Equations (40) are linear on both sides of the flame. Their solution contains eight constants, which are determined from any eight conditions of the nine conditions given by Eqs. (42) and (44). The last ninth condition provides the solvability condition,

$$\mathcal{G}(\lambda; m, q, \ell, b, Le_Z, Le_F) = 0\,, \tag{46}$$

which was used to calculate λ. Remember that the steady state flame position, x_{f0}, is already a function of the other parameters and therefore is not included in the argument list for $\mathcal{G}$. As in the case of steady-state solutions, it seems impossible to write down Eq. (46) explicitly because of its length. However, the existence of an analytical and explicit expression allows us to investigate the presence or absence of eigenvalues of the problem in the right half-plane of the complex λ-plane.

Function $\mathcal{G}$ is complex for complex λ values. Estimating numerical values of $\mathcal{G}$ showed that the eigenvalues appear in the right half-plane only on the $\lambda_I = 0$ axis, at least for the cases considered in this work. Figure 11 illustrates this.

The left plot of Fig. 11 shows the contours of zero values of the real (solid lines) and complex (dashed line) parts of the function $\mathcal{G}$ evaluated for $\ell = 100$, $m = 2$, $b = 0.5$, $Le_F = 1$, $Le_Z = 0.3$ and various x_f near the turning point. The dependence of x_f on q for the same parameter values is shown in the right plot of Fig. 11, where the cases of the x_f values from the right plot are marked with small circles.

It can be seen that for $x_f = 48$ (the value below the turning point) the solid and dashed lines do not intersect and, thus, there are no eigenvalues in the right half-plane of λ. For this set of parameters, the turning point is situated approximately at $x_f \approx 49$. For this value, the solid and dashed lines intersect at the point $\lambda = 0$. For larger x_f values (above the turning point, the curves plotted for $x_f = 50$), the solid and dashed lines intersect at $\lambda_R > 0$ and $\lambda_I = 0$. Plots of $\mathcal{G}_R$ versus λ_R along the real axis are shown in Fig. 12, where zero values are marked with small circles. A similar dependence for the eigenvalues in the right half-plane was observed for other values of the parameters.

Thus, we can conclude that in the presence of two steady-state solutions, the solution corresponding to a larger value of x_f is unstable. The instability is monotonous in nature. When x_f crosses the turning point, the eigenvalue $\lambda = 0$ appears. This eigenvalue moves to the right half of the complex plane with a further increase of x_f and remains purely real. No oscillatory instabilities ($\lambda_I \neq 0$) were found, at least for the considered range of parameters.

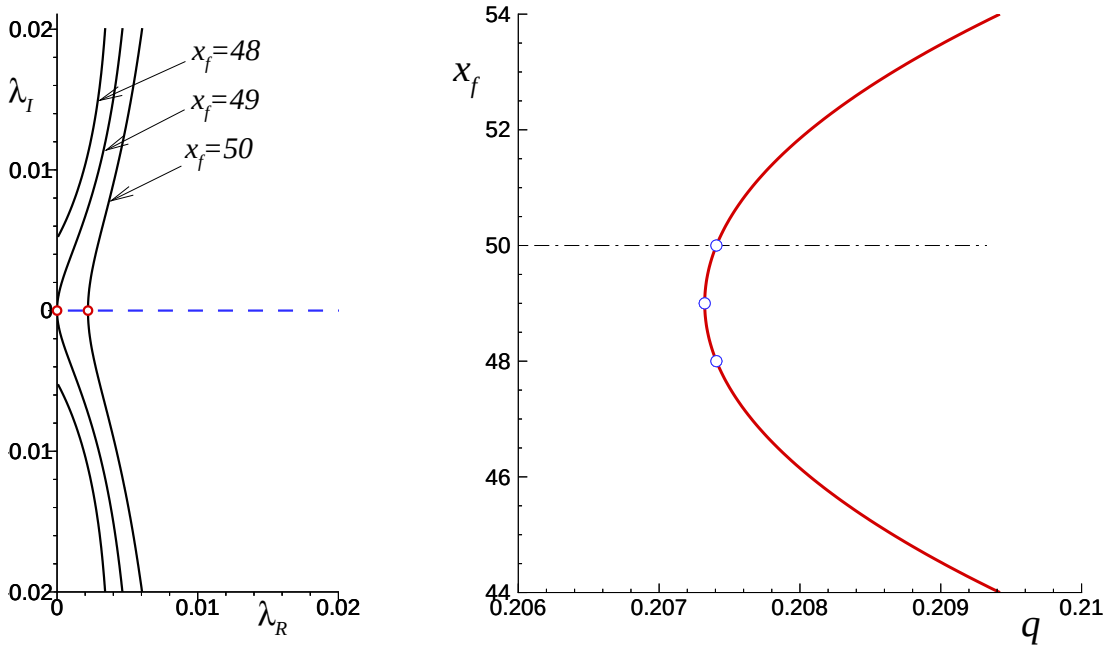

Figure 11: Left plot: Example of zeroth isolines of the real (solid lines) and imaginary (a dashed line) parts of $\mathcal{G}$ given by Eq. (46) and plotted for $\ell = 100$, $m = 2$, $b = 0.5$, $Le_F = 1$ $Le_Z = 0.3$ and various x_f. Small circles indicate the eigenvalues λ. Right plot: dependence of x_f versus q for the same parameter values. Small circles indicate the cases of x_f shown in the left plot.

6 Comparison of analytical and finite-β solutions

It is interesting to compare the analytical HAEA results obtained in Section 3 and those for finite Zel'dovich numbers. For this, the steady-sate counterpart of Eqs. (2)-(5) was calculated applying the Gauss-Seidel method with over-relaxation. Before doing the comparison, it is necessary to make the following remarks.

At finite β, the value of the critical heat of reaction for the flammability limit, q_f, depends on Le_z and γ being $q_f \to 1$ for $\beta \to \infty$, see [41]. The calculation of this limit was done using the planar flame propagation velocity as a small parameter. The dimensionless chain-branching temperature also falls below unity at finite β values.

When obtaining analytical solutions for the HAEA limit, the position of the flame was defined as a point where $\theta_1 = 1$. This is the point at which the δ-function is located replacing

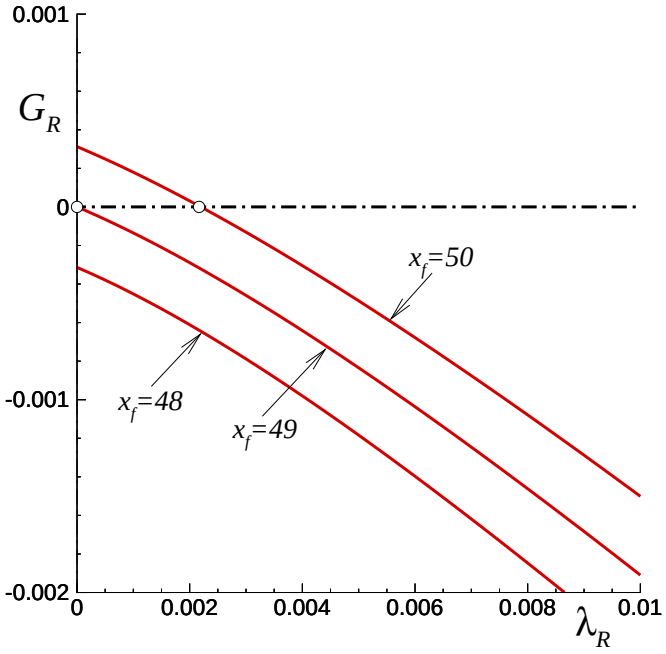

Figure 12: Dependencies of $\mathcal{G}_R$ on λ_R along the real axis; zero values are marked with small circles.

the spatially distributed reaction rate ω given by Eq. (14). It coincides with the point of the maximum mass fraction value of radicals Z. But in the case of β finite, this does not happen. The points where the temperature is equal to unity and where the mass fraction of radicals has a maximum value coincide only in the HAEA limit. All this can lead to the fact that the point with $\theta_1 = 1$ may not exist in some cases, when the θ_1 remains less than unity, and the only way to characterize the flame position is the point where Z reaches its maximum.

The spatial distributions of quantities calculated for $\beta = 10$, $\ell = 50$, $b = 0.5$, $\gamma = 0.7$ are illustrated in Fig. 13 for the case of isothermal (cold) conditions outside the heat-exchange segment. For the case with $q = 0.5789$ (upper plot), the value of $\theta_1 = 1$ is reached and is marked with a small open circle. For the case with $q = 0.4139$ (lower figure), the temperature in the first channel never reaches the value $\theta_1 = 1$.

Figure 14 compares the flame position x_f versus the dimensionless heat of reaction q obtained for finite and infinite β values. The solid line shows the analytical HAEA results using the points with $\theta_1 = 1$. The dashed, dash-dotted and long-dash lines represent the numerical

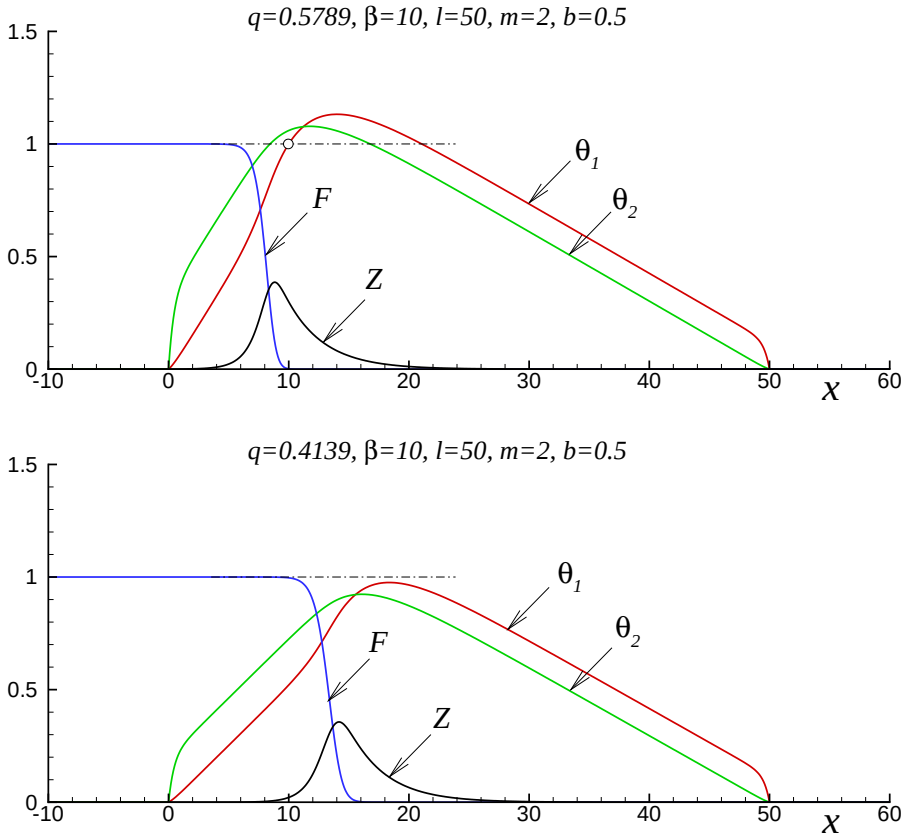

Figure 13: Spatial distributions of temperature, fuel mass fraction and radicals mass fraction calculated for $\beta = 10$, $\ell = 50$, $b = 0.5$, $\gamma = 0.7$, $Le_Z = 0.7$ and $Le_F = 1$ and two values of q, marked in Fig.14 with vertical arrows facing the axis q.

curves calculated for $\beta = 20$, 10 and 5, respectively, drawn using the points where the mass fraction of radicals is maximum. As indicated above, near the turning point $q = q_{min}$ the value with $\theta_1 = 1$ is not reached anymore. Small triangles indicate the positions of these points ($\theta_1 = 1$) plotted for $\beta = 10$ when they are reached.

One can see in this figure that the curves tend to converge as β increases, as it should be. We can also note that, to some extent, the difference observed for finite and infinite Zel'dovich numbers is due to the different methods used for determining the flame position, as described above. When the points with $\theta_1 = 1$ exist at finite β (shown with small triangles in Fig. 14 for $\beta = 10$), they are noticeably closer to the asymptotic curve than points corresponding to the maximum of Z.

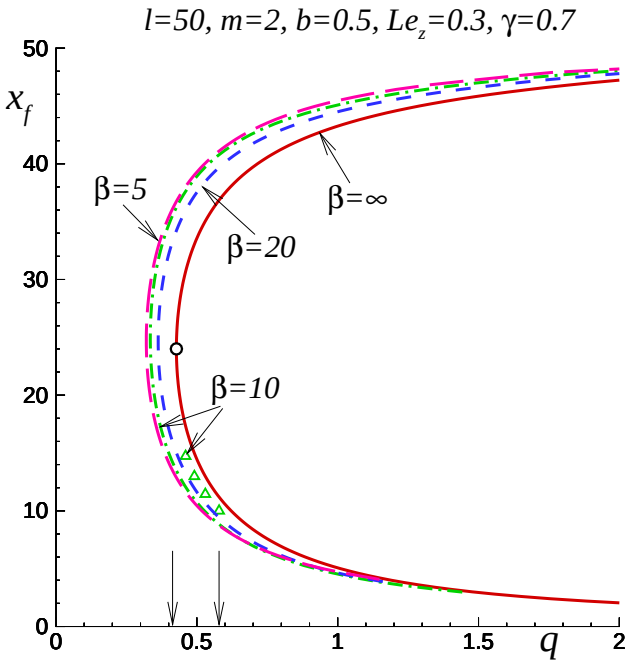

Figure 14: Comparison of the flame positions x_f for finite (dashed, dash-dotted and long-dash lines for $\beta = 20$, 10, and 5, respectively, defined as a maximum of Z) and infinite (solid curve, defined as $\theta_1 = 1$) Zel'dovich numbers; small triangles show the points where $\theta_1 = 1$ for $\beta = 10$ when they exist. The two vertical arrows pointing downward indicate the cases shown in Fig. 13.

7 Discussion and conclusions

Advances in computing power have qualitatively changed the understanding of combustion processes in the last decades. Numerical simulations for 2D and 3D problems with complex chemical kinetics are already becoming commonplace for researchers. However, in this regard, a significant increase in the possibilities for constructing analytical solutions by means of computing facilities, and their application to combustion problems, often remains unappreciated. On the other hand, the analytical solutions not only bring clarity to the understanding of complex processes, but also serve as a reliable basis for verifying purely numerical results.

Still, some similarities between modern numerical and analytical approaches to problem solving should be noted. As for numerical procedures, detailed presentation of analytical results to a reader may not be possible in some cases, mainly due to their length. On the other hand,

extremely long expressions for analytical formulae hardly bring a greater understanding of the phenomena being studied. However, the existence of an analytical expression, even without the possibility of being presented to a reader, opens up much greater opportunities for a parametric analysis of the problem, since this no longer includes intrinsic numerical parameters, such as the grid spacing, or the degree of convergence of the results, for example.

In the present work, the study of combustion of ultra lean mixtures in superadiabatic devices of the counterflow type is presented. A chemistry model with two-step kinetics within which the flammability limit appears explicitly was chosen. The existence of a planar adiabatic combustion front was taken as the fundamental flammability criterion. The investigation is carried out on the basis of analytical solutions; this becomes possible in the HAEA limit when the autocatalytic reaction rate is replaced by the Dirac δ-function. As a model of the device, a simplified shape was chosen in the form of narrow channels through which the gas flows in a counterflow regime and the heat exchange between the channels is carried out over a finite wall length.

The analysis of the obtained solutions showed that the total number of steady-state modes with combustion in the system can be up to two, and if we include the cold mode (without reaction), then up to three. It should also be noted that one of the combustion modes is always unstable.

The parametric study of the obtained solutions showed that the main parameters for the device operation are the length of the heat-exchange segment and the effective heat-exchange coefficient between the channels. It has been shown that for virtually any mixture, including lean ones and those below the standard flammability limit, an increase in the length of the heat exchange segment to a sufficient large value provides a feasible combustion process. A similar conclusion can be made about the effective coefficient of heat exchange between the channels, that is, an increase in this parameter to a sufficiently large value ensures stable combustion for any lean mixture. However, an increase in this parameter can be limited by the thermo-physical properties of the device material.

Nevertheless, it should be noted that within the model under consideration, the heat-losses from the combustion zone to the external environment were neglected. The inclusion of this effect into consideration will possibly limit the lower value for the initial fuel mass fraction above which a stable combustion process is possible.

Acknowledgement

This work was financed by project #PID2019-108592RB-C42 / AEI / 10.13039/501100011033.

Appendix. Conditions of limit burning

For the sake of completeness, we consider below the limiting flammability conditions appearing in the HAEA limit, that we define as the value of q below which a planar adiabatic freely propagating flame can not exist. The governing equations describing the flame front with heat losses neglected steadily propagating with the velocity m are

$$\begin{cases} mF^I = Le_F^{-1} F^{II} - m\delta(x - x_f)\,, \\ mZ^I = Le_Z^{-1} Z^{II} - Z + m\delta(x - x_f)\,, \\ m\theta^I = \theta^{II} + qZ\,. \end{cases} \tag{47}$$

These equations are to be solved separately for $x < x_f$ and $x > x_f$. The nonlinear term describing the rate of radical formation is replaced by a δ-function with a factor obtained by integrating the F-equation over x from $-\infty$ to ∞. The boundary conditions in the distance become

$$x \to -\infty: \quad \theta = F - 1 = Z = 0; \quad x \to \infty: \quad \theta^I = F^I = Z = 0\,. \tag{48}$$

Without limitations, the combustion front is fixed at $x_f = 0$. The solutions for F and Z functions are identical to those of Eqs. (21)-(22). For the temperature field, one can get

$$\theta = \begin{cases} \left(1 - \dfrac{qZ_f}{ma_m - a_m^2}\right) e^{mx} + \dfrac{qZ_f}{ma_m - a_m^2}\, e^{a_m x} & x < 0\,, \\ \left(1 - \dfrac{qZ_f}{ma_p - a_p^2}\right) + \dfrac{qZ_f}{ma_p - a_p^2}\, e^{a_p x} & x > 0\,, \end{cases} \tag{49}$$

where a_m, a_p and Z_f are given by Eqs. (23)-(24). Substitution of Eq. (49) into the condition of continuity of the temperature derivative across $x = 0$ gives the relation to determine the wave speed, m, in an implicit form

$$q = \frac{m}{Z_f} \left\{ \frac{m - a_m}{ma_m - a_m^2} + \frac{a_p}{ma_p - a_p^2} \right\}^{-1}. \tag{50}$$

This function is shown in Fig. 15 (left plot) for different Le_Z.

Combustion in a planar front corresponds to $m > 0$. It can be seen from Eq. (50) that $q \to 1$ as $m \to 0$ for any Lewis numbers. For $m < 0$, the solution takes on a non-physical nature. Thus, $q_f = 1$ represents the limiting condition for the planar combustion wave front as $\beta \to \infty$.

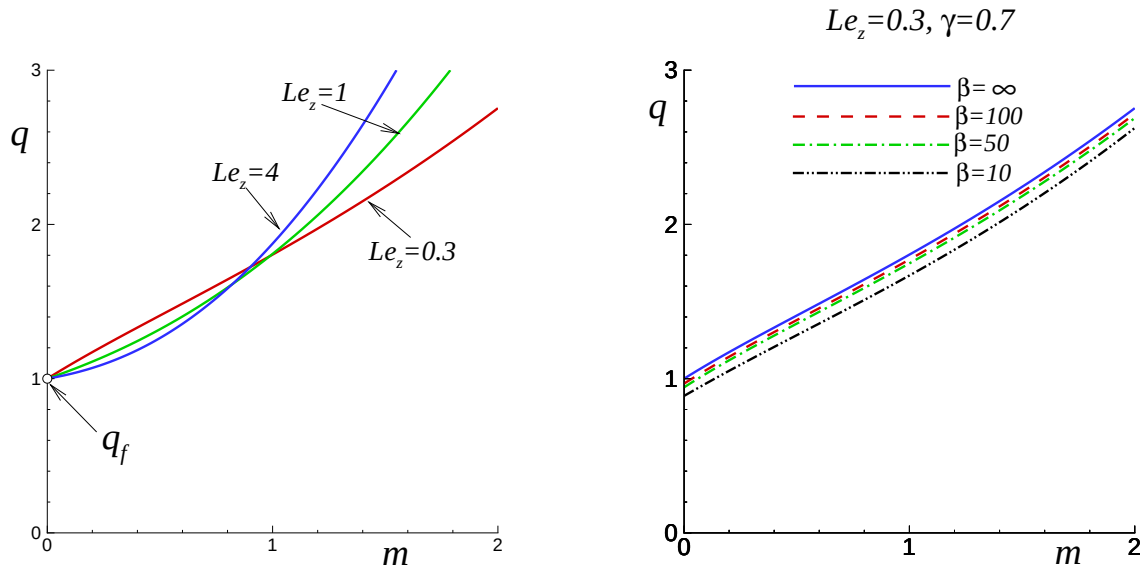

Figure 15: Left plot: the dependence of q versus m for a planar adiabatic combustion front calculated for $\beta \to \infty$ from Eq. (50). The combustion wave exists for $m > 0$. The flammability limit value, $q_f = q(m \to 0)$, results to be 1 for any Le_Z and there are no physical solutions for $q < 1$. Right plot: the dependence of q versus m obtained numerically for varying β.

The critical conditions for the combustion front existence, namely the limiting values of q_f representing the flammability limit, were obtained asymptotically for finite values of β in [41]. In that study the velocity of the flame front propagation was taken as a small parameter and an implicit algebraic expression determining q_f as a function of parameters was obtained. The right plot of Fig. 15 shows the dependencies q on m obtained numerically for various increasing β values. It can be seen that a very close approximation to the asymptotic curve for $\beta \to \infty$ is observed only at very large (may be non-physical) values of the order of a hundred, while at more physical values, $\beta = O(10)$, the approaching of the curves to the asymptotic one is only satisfactory. One can also see that at finite β, the flammability limit values, q_f for $m \to 0$, turn out to be less than the unit value obtained for $\beta \to \infty$.

The existence of the standard flammability limits can also be understood by means of the first integral of Eqs. (47)-(48)

$$m[\theta + q(Z + F - 1)] = \frac{d}{dx}\left[\theta + q\left(\frac{F}{Le_F} + \frac{Z}{Le_Z}\right)\right]. \tag{51}$$

With complete combustion of fuel, $F(x \to \infty) = 0$, we have $\theta(x \to \infty) = q$. And if $q < 1$, the

branching temperature ($\theta = 1$) can never be reached within the HAEA limit. We mention again, that at finite β the critical value for q is slightly below unity, see [41].

References

[1] A.C. Fernández-Pello, Micropower generation using combustion: issues and approaches, *Proc. Combust. Inst.* 29 (2002) 883-899.

[2] D. Dunn-Rankin, E.M. Leal , D.C. Walther, Personal power systems, *Prog. Energy Combust. Sci.* 31 (2005) 422-465.

[3] Y. Ju, K. Maruta, Microscale combustion: technology development and fundamental research, *Prog. Energy Combust. Sci.* 37 (2011) 669-715 .

[4] D.C. Walther, J. Ahn, Advances and challenges in the development of power-generation systems at small scales, *Prog. Energy Combust. Sci.* 37 (2011) 583-610 .

[5] K. Maruta, Micro and mesoscale combustion, *Proc. Combust. Inst.* 33 (2011) 125-150.

[6] N.S. Kaisare, D.G. Vlachos, A review on microcombustion: fundamentals, devices and applications, *Prog. Energy Combust. Sci.* 38 (2012) 321-359.

[7] J.L. Ellzey, E.L. Belmont, C.H. Smith, Heat recirculating reactors: Fundamental research and applications, *Prog. Energy Combust. Sci.* 72 (2019) 32-58.

[8] S.A. Lloyd, F.J. Weinberg, A burner for mixtures of very low heat content, *Nature* 251 (1974) 47-49.

[9] S.A. Lloyd, F.J. Weinberg, Limits to energy release and utilisation from chemical fuels, *Nature* 257 (1975) 367-370.

[10] A.R. Jones, S.A. Lloyd, F.J. Weinberg, Combustion in heat exchangers, *Proc. R. Soc. Lond. A.* 360 (1978) 97-115.

[11] P. Ronney, Analysis of non-adiabatic heat-recirculating combustors, *Combust. Flame* 135 (2003) 421-439.

[12] Y. Ju, C.W. Choi, An analysis of sub-limit flame dynamics using opposite propagating flames in mesoscale channels, *Combust. Flame* 133 (2003) 483-493.

[13] R.V. Fursenko, S. S. Minaev, Flame stability in a system with counterflow heat exchange, *Combust. Explos. Shock Waves* 41(2) (2005) 133-139.

[14] I. Schoegl, J.L. Ellzey, Superadiabatic combustion in conducting tubes and heat exchangers of finite length, *Combust. Flame* 151 (2007) 142-159.

[15] J.A. Federici, D.G. Vlachos, A computational fluid dynamics study of propane/air microflame stability in a heat recirculation reactor, *Combust. Flame* 153 (2008) 258-269.

[16] I.M. Schoegl, J.L. Ellzey, Numerical investigation of ultra-rich combustion in counter-flow heat exchangers, *Combust. Sci. Technol.* 182 (2010) 1413-1428.

[17] V.N. Kurdyumov, M. Matalon, Analysis of an idealized heat-recirculating microcombustor, *Proc. Combust. Inst.*, 33(2) (2011) 3275-3284.

[18] M. Sánchez-Sanz, Premixed flame extinction in narrow channels with and without heat recirculation, *Combust. Flame* 159 (2012) 3158-3167.

[19] E.L. Belmont, P. Radyjowski, J. L. Ellzey, Effect of geometric scale on heat recirculation and syngas production in a noncatalytic counter-flow reformer, *Combust. Sci. Technol.* 187 (2015) 874-893.

[20] E. Fernández-Tarrazo, M. Sánchez-Sanz, R. Fursenko, S. Minaev, Multiple combustion regimes and performance of counter-flow microcombustor with power extraction, *Math. Modell. Nat. Phen.* 13 (2018) UNSP 52.

[21] D. Fernández-Galisteo, E. Fernández-Tarrazo, C. Jiménez, V.N. Kurdyumov, Analysis of an idealized counter-current microchannel-based reactor to produce hydrogen-rich syngas from methanol, *Int. J. Hydr. Eng.* 44 (2019) 23807-23820.

[22] V.N. Kurdyumov, D. Fernández-Galisteo, C. Jiménez, Superadiabatic small-scale combustor with counter-flow heat exchange: Flame structure and limits to narrow-channel approximation, *Combust. Flame* 222 (2020) 233-241.

[23] D.J Diamantis, E. Mastorakos, D.A. Goussis, Simulations of premixed combustion in porous media, *Combust. Theory Modell.* 6 (2002) 383411.

[24] F.M. Pereira, A.A.M. Oliveira, F.F. Fachini, Theoretical analysis of ultra-lean premixed flames in porous inert media, *J. Fluid Mech.* 657 (2010) 285-307.

[25] P.-A. Masset, O. Dounia, L. Selle, Fully explicit formulae for flame speed in infinite and finite porous media, *Combust. Theory Modell.* 2021, https://doi.org/10.1080/13647830.2021.1939422

[26] Ya.B. Zeldovich, K teorii rasprostranenia plameni, *Zh. Fiz. Khim.* 22 (1948) 27-48; Theory of flame propagation, English translation: *Nat. Advis. Comm. Aeronaut.* Technical Memorandum No. 1282, 1951.

[27] Ya.B. Zeldovich, Chain reactions in hot flames - an approximate theory for flame velocity, *Kinetika i kataliz* 2 (1961) 305-318; English translation: *Int. Chem. Eng.* 2 (1962) 227-235.

[28] Ya.B. Zeldovich, G.I. Barenblatt, V.B. Librovich, G.M. Mahviladze, *The mathematical Theory of Combustion and Explosions*, Consultants Bureau, New York, 1985.

[29] A. Liñán, A theoretical analysis of premixed flame propagation with an isothermal chain-branching reaction, Insituto Nacional de Technica Aerospacial Esteban Terradas (Madrid), USAFORS Contract No. E00AR68-0031, Technical Report No. 1, 1971.

[30] G. Joulin, A. Liñán, G.S.S. Ludford, N. Peters, C. Schmidt-Laine, Flames with chain-branching/chain-breaking kinetics, *SIAM J. Appl. Math.* 45 (1985) 420-434.

[31] J.W. Dold, R.W. Thatcher, A. Omon-Arancibia, J. Redman, From one-step to chain-branching premixed flame asymptotics, *Proc. Combust. Inst.* 29 (2002) 1519-1526.

[32] J.W. Dold, R.O. Weber, R.W. Thatcher, A.A. Shah, Flame balls with thermally sensitive intermediate kinetics, *Combust. Theory Modell.* 7 (2003) 175-203.

[33] J.W. Dold, J. Daou, R.O.Weber, Reactive-diffusive stability of planar flames with modified Zeldovich-Liñán kinetics, in "Simplicity, Rigor and Relevance in Fluid Mechanics. A volume in honor of Amable Liñán", Edited by F.J. Higuera, J. Jiménez, and J.M. Vega, eds., CIMNE, Barcelona, 2004.

[34] J.W. Dold, Premixed flames modelled with thermally sensitive intermediate branching kinetics, *Combust. Theory Modell.* 11 (2007) 909-948.

[35] V.V. Gubernov, H.S. Sidhu, G.N. Mercer, Combustion waves in a model with chain branching reaction and their stability, *Combust. Theory Modell.* 12 (2008) 407-431.

[36] V.V. Gubernov, H.S. Sidhu, G.N. Mercer, A.V. Kolobov, A.A. Polezhaev, The effect of Lewis number variation on combustion waves in a model with chain-branching reaction, *Math. Chem.* 44 (2008) 816-830.

[37] V.V. Gubernov, A.V. Kolobov, A.A. Polezhaev, H.S. Sidhu, G.N. Mercer, Pulsation instabilities of combustion waves in a chain-branching reaction model, *I. J. Bif. Chaos* 19 (2009) 873-887.

[38] G.J. Sharpe, Effect of thermal expansion on the linear stability of planar premixed flames for a simple chain-branching model: The high activation energy asymptotic limit, *Combust. Theory Modell.*, 12 (2008) 717-738.

[39] G.J. Sharpe, Thermal-diffusive instability of premixed flames for a simple chain-branching chemistry model with finite ectivation energy, *SIAM J. Appl. Math.* 70 (2009) 866-884.

[40] V.V. Gubernov, A.V. Kolobov, A.A. Polezhaev, H.S. Sidhu, Stability of combustion waves in the Zeldovich-Liñán model, *Combust. Flame* 159 (2012) 1185-1196.

[41] V.N. Kurdyumov, D. Fenández-Galisteo, Asymptotic structure of premixed flames for a simple chain-branching chemistry model with finite activation energy near the flammability limit, *Combust. Flame* 159 (2012) 3110-3118.

[42] H. Zhang, Z. Chen, Bifurcation and extinction limit of stretched premixed flames with chain-branching intermediate kinetics and radiative loss, *Combust. Theor. Modell* 22 (2018) 531-553.

[43] V.V. Gubernov, V.I. Babushok, S.S. Minaev, Phenomenological model of chain-branching premixed flames, *Combust. Theor. Modell* 23 (2019) 261-278.

[44] D. Fernández-Galisteo, A.L. Sánchez, A. Liñán, F.A. Williams, The hydrogen-air burning rate near the lean flammability limit, *Combust. Theory Modell.* 13 (2009) 741-761.

[45] D. Fernández-Galisteo, A.L. Sánchez, A. Liñán, F.A. Williams, One-step reduced kinetics for lean hydrogen-air deflagration, *Combust. Flame* 156 (2009) 985-996.

[46] D. Fernández-Galisteo, A. Weiss, A.L. Sánchez, F.A. Williams, A one-step reduced mechanism for near-limit hydrogen combustion with general stoichiometry, *Combust. Flame* 208 (2019) 1-4.

[47] A.L. Sánchez, F.A. Williams, Recent advances in understanding of flammability characteristics of hydrogen, *Prog. Eng. Combust. Sci.* 41 (2014) 1-55.

[48] A.H. Nayfeh, Perturbation Methods, Wiley & Sons, Inc., 1973.